# Dipole oscillation modes in light $\alpha$-clustering nuclei

W. B. He (何万兵),[1,2] Y. G. Ma (马余刚),[1,3,*] X. G. Cao (曹喜光),[1,†] X. Z. Cai (蔡翔舟),[1] and G. Q. Zhang (张国强)[1]

[1]*Shanghai Institute of Applied Physics, Chinese Academy of Sciences, Shanghai 201800, China*

[2]*University of the Chinese Academy of Sciences, Beijing 100080, China*

[3]*ShanghaiTech University, Shanghai 200031, China*

(Received 8 March 2016; revised manuscript received 14 May 2016; published 5 July 2016)

The $\alpha$ cluster states are discussed in a model frame of extended quantum molecular dynamics. Different $\alpha$ cluster structures are studied in detail, such as $^{8}$Be two-$\alpha$ cluster structure, $^{12}$C triangle structure, $^{12}$C chain structure, $^{16}$O chain structure, $^{16}$O kite structure, and $^{16}$O square structure. The properties studied include the width of wave packets for different $\alpha$ clusters, momentum distribution, and the binding energy among $\alpha$ clusters. We also discuss how the $\alpha$ cluster degree of freedom affects nuclear collective vibrations. The cluster configurations in $^{12}$C and $^{16}$O are found to have corresponding characteristic spectra of giant dipole resonance (GDR), and the coherences of different $\alpha$ clusters' dipole oscillations are described in detail. The geometrical and dynamical symmetries of $\alpha$-clustering configurations are responsible for the number and centroid energies of peaks of GDR spectra. Therefore, the GDR can be regarded as an effective probe to diagnose different $\alpha$ cluster configurations in light nuclei.

DOI: 10.1103/PhysRevC.94.014301

## I. INTRODUCTION

Clustering is a fundamental physics aspect in lighter nuclei ($Z \leqslant 16$), where the mean field effect is not strong enough to break cluster formation at low temperatures. It is typically observed as excited states of those nuclei and also in the ground states of nuclei far from the $\beta$ stability line, where nuclei can behave like molecules composed of nucleonic clusters. Many authors have focused on clustering in recent decades [1,2]. Near the threshold of decay into the subunit, nuclei can be assumed to change into molecule-like structures [3]. Due to the high stability of the $\alpha$ particle, the $2n$-$2p$ correlation plays a critical role in light nuclei clustering. The self-conjugate light nuclei are expected to have a phase change in which nucleons condense into $\alpha$ particles as the density becomes lower than one third of the normal nuclear matter density [4]. As the density falls to one fifth of normal nuclear matter, the self-conjugate light nuclei are expected to be in an $\alpha$-gas or a Bose condensed state [5]. In neutron rich light nuclei, nuclear molecules with clusters bound via neutrons can show up, at low density [2]. As the density decreases, $\alpha$ clustering will dramatically change the nuclear equation of state [6–10]. The famous Hoyle state in $^{12}$C at 7.65 MeV, which is considered a key point of the $^{12}$C synthesis in the Universe, is believed to be formed out of a weakly interacting gas of $\alpha$ particles [11]. However, many issues are not yet well understood, such as how $\alpha$ clustering determines the configurations and shapes of the many-body system, what are the underlying mechanism and collective dynamics of $\alpha$-clustering systems, etc. [12–16].

Since its discovery, giant dipole resonances (GDR) has been revealed in nuclei as light as $^{4}$He [17] and as heavy as $^{232}$Th [18]. Therefore, GDR is a good tool for systematical investigation of collective properties throughout the nuclear chart. As the most pronounced feature of excited nuclei, GDR can give crucial clues to understand nuclear structure and collective dynamics. The centroid energy of GDR can provide direct information about nuclear size and the nuclear equation of state [19]. Meanwhile, the GDR width can be used as a direct experimental probe to measure the nuclear deformation at finite temperature and angular momentum over the entire mass region [20,21]. The GDR strength has a single peak distribution for spherical nuclei with mass number $>60$. However, the GDR strength usually shows configuration splitting in light nuclei [19,22–24]. In light nuclei with molecule-like structures, the deformation is huge enough to cause big splitting of GDR. In addition, the degree of freedom of clusters in nuclei affects the GDR spectra. Multifragmented peaks can be expected for self-conjugate ($\alpha$) nuclei with a prominently developed $\alpha$ cluster structure in excited states. A recent study by Chiba *et al.* found that asymmetric cluster configurations in $\alpha$ conjugate nuclei contribute to resonances by isoscalar dipole transition at relatively small excitation energy [25]. Therefore, it is interesting to study how an $\alpha$ cluster component manifests itself in GDRs. The GDR spectra will provide important and direct information to reveal the geometrical configurations and dynamical interactions among $\alpha$ clusters.

Configurations of $\alpha$ clusters are a key problem to understand the clustering in light nuclei. Theoretical predictions made recently on $\alpha$ cluster configuration in light nuclei revealed the following aspects. $^{8}$Be composed of two $\alpha$ particles has a scarcely greater value than the threshold energy for the decay into two $\alpha$ particles [3]. For $^{12}$C, a triangular-like configuration is predicted around the ground state by Fermionic molecular dynamics [26], antisymmetrized molecular dynamics [27,28], and covariant density functional theory [29], which is supported by a recent experimental result [30]. A three-$\alpha$ linear-chain configuration was predicted as an excited state in time-dependent Hartree-Fock theory [12], and other different approaches [31]. In the framework of the cranking covariant

*ygma@sinap.ac.cn

†caoxiguang@sinap.ac.cn

 

density functional theory, the mechanisms to stabilize a linear-chain configuration were discussed in detail [32]. The intrinsic density of $^{12}$C and $^{16}$O may display a localized linear-chain density profile as an excitation of the condensed gas-like states described with the Brink wave function and the Tohsaki-Horiuchi-Schuck-Röpke (THSR) wave function [5,33,34]. For $^{16}$O, the linear-chain structure with four $\alpha$ clusters was supported by the $\alpha$ cluster model [35] and the cranked Skyrme Hartree-Fock method [13]. A tetrahedral structure of $^{16}$O, made out of four $\alpha$ clusters, is found above the ground state with the constrained Hartree-Fock-Bogoliubov approach [6]. However, recent calculations with nuclear chiral effective field theory [36] and covariant density functional theory [29] support the tetrahedral $\alpha$ configuration located at the ground states. An algebraic model [37] shows that the ground-state rotational band supporting the nucleus has tetrahedral symmetry. Orthogonality condition model calculations show a duality of the mean-field-type as well as $\alpha$-clustering character in the $^{16}$O ground state [38]. There are different configuration descriptions implying the $\alpha$ cluster structure in $^{20}$Ne and $^{24}$Mg, such as three-dimensional shuttle shape [6,14] or chain states [39,40] and nonlocalized cluster states [41]. Therefore, it is important to look for new experimental probes to diagnose different configurations of $\alpha$ conjugate nuclei around the cluster decay threshold [42].

In this work, we report our results of GDRs of $\alpha$ cluster states of $^{8}$Be, $^{12}$C, and $^{16}$O within a microscopic dynamical many-body approach. First, we discuss the method of GDR calculations within QMD models. Then by demonstrating the results of $^{12}$C and $^{16}$O in the ground states, we show the reliability of GDR calculations in our model, and propose the coexistence of triangle shape and spherical shape in $^{12}$C ground states. Finally, we investigate how the different $\alpha$ configurations lead to multifragmented peaks of GDR and the underlying mechanism which is responsible for the collective motion of $\alpha$-clustering light nuclei reported in our previous publication [24].

## II. MODEL AND METHODOLOGY

### A. Model introduction

Quantum molecular dynamics (QMD), a powerful tool for studying intermediate energy nuclear reactions and nuclear fragmentation [43], has been successfully applied in studies of giant dipole resonance (GDR), pygmy dipole resonance (PDR), and giant monopole resonance (GMR) due to its microscopic basis and high flexibility [28,44–47]. In the following calculations of GDRs, the nuclear system is described within the QMD model framework. To apply this approach to light nuclei such as $^{8}$Be, $^{12}$C, and $^{16}$O, some requirements for the model are necessary. For example, the energy and radius of ground states must be well described, and the ground states must be stable enough. Nevertheless, standard QMD shows insufficient stability because the initialized nuclei are not in their real ground states. In this paper, we use an extended QMD (EQMD) with some new features [48,49]. It is introduced briefly as follows.

In EQMD, nucleons are treated as Gaussian wave packets $\varphi_i$, which are written as

$$\varphi_i(\mathbf{r}_i) = \left(\frac{v_i + v_i^*}{2\pi}\right)^{3/4} \exp\left[-\frac{v_i}{2}(\mathbf{r}_i - \mathbf{R}_i)^2 + \frac{i}{\hbar}\mathbf{P}_i \cdot \mathbf{r}_i\right], \tag{1}$$

where $v_i = 1/\lambda_i + i\delta_i$ is width of the complex Gaussian wave packets. $\lambda$ and $\delta$ are dynamic variables. The $v_i$ of Gaussian wave packets for each nucleon is dynamic and independent. This is an important improvement compared with standard QMD, in which a uniform and static width is applied for all nucleons. Dynamical wave-packet width not only improves the capability of describing the ground state, but also helps to describe nuclear exotic structures, such as nuclear halo structure. Furthermore, the kinetic-energy term arising from the momentum variance of wave packets is taken into account by subtracting the spurious zero-point center-of-mass (c.m.) kinetic energy from the Hamiltonian. This procedure is important for QMD models to describe nuclear cluster states and fragmentation. In standard QMD, the kinetic-energy term arising from the momentum variance of wave packets is constant. Thus, the constituent nucleons having finite momenta are not in energy-minimum states, hence the source of insufficient stability. So, the Hamiltonian can be written as

$$\begin{aligned} H &= \langle\Psi|\sum_i -\frac{\hbar^2}{2m}\nabla_i^2 - \widehat{T}_{\text{c.m.}} + \widehat{H}_{\text{int}}|\Psi\rangle \\ &= \sum_i \left[\frac{\mathbf{P}_i^2}{2m} + \frac{3\hbar^2\left(1+\lambda_i^2\delta_i^2\right)}{4m\lambda_i}\right] - T_{\text{c.m.}} + H_{\text{int}}, \end{aligned} \tag{2}$$

where $T_{\text{c.m.}}$ is the term of zero-point center-of-mass (c.m.) kinetic energy, the form of which can be found in detail in Ref. [48]. For the effective interaction, Skyrme and Coulomb forces, the symmetry energy, and the Pauli potential are used:

$$H_{\text{int}} = H_{\text{Skyrme}} + H_{\text{Coulomb}} + H_{\text{Symmetry}} + H_{\text{Pauli}}. \tag{3}$$

The form of Skyrme interaction use in EQMD model is the simplest, written as

$$H_{\text{Skyrme}} = \frac{\alpha}{2\rho_0}\int \rho^2(\mathbf{r})d^3r + \frac{\beta}{(\gamma+1)\rho_0^\gamma}\int \rho^{\gamma+1}(\mathbf{r})d^3r, \tag{4}$$

where $\alpha = -124.3$ MeV, $\beta = 70.5$ MeV, and $\gamma = 2$. The symmetry potential is written as

$$H_{\text{Symmetry}} = \frac{C_S}{2\rho_0}\sum_{i,j\neq i}\int [2\delta(T_i,T_j) - 1]\rho_i(\mathbf{r})\rho_j(\mathbf{r})d^3r, \tag{5}$$

where $C_S$ is the symmetry energy coefficient and here $C_S =$ 25 MeV. Specifically, the Pauli potential is written as

$$H_{\text{Pauli}} = \frac{c_P}{2}\sum_i (f_i - f_0)^\mu \theta(f_i - f_0), \tag{6}$$

$$f_i \equiv \sum_j \delta(S_i,S_j)\delta(T_i,T_j)|\langle\phi_i|\phi_j\rangle|^2, \tag{7}$$

where $f_i$ is the overlap of a nucleon $i$ with nucleons having the same spin and isospin; $\theta$ is the unit step function; $c_P$ is a coefficient related to strength of the Pauli potential. This potential inhibits the system from collapsing into the Pauli-blocked state at low energy and gives the model the capability to describe $\alpha$ clustering. This capability is crucial to our calculation because it enables the GDR study on $\alpha$ cluster configurations. Since the clustering configurations and the profiles of GDR spectra are not sensitive to different forms of potential, the relation between clustering configurations and GDR spectra is independent of EQMD model. The phase space of nucleons is obtained initially from a random configuration. To get the energy-minimum state as a ground state, a frictional cooling method is used for the initialization process. The model can describe quite well the ground state properties, such as binding energy, rms radius, deformation, etc., over a wide mass range [50].

### B. GDR algorithm

The macroscopic description of GDR by the Goldhaber-Teller model [51] assumes that protons and neutrons collectively oscillate with opposite phases in an excited nucleus. In the EQMD model, the location and momentum of all nucleons are explicit variables. Based on the Goldhaber-Teller assumption, we can calculate the oscillation energy spectra. The dipole moments of the system in coordinate space $D_G(t)$ and momentum space $K_G(t)$ are defined as follows [45,46,52]:

$$D_G(t) = \frac{NZ}{A}[R_Z(t) - R_N(t)], \tag{8}$$

$$K_G(t) = \frac{NZ}{A\hbar}\left[\frac{P_Z(t)}{Z} - \frac{P_N(t)}{N}\right], \tag{9}$$

where, $R_Z(t)$ and $R_N(t)$, and $P_Z(t)$ and $P_N(t)$, are the centers of mass of the protons and neutrons in coordinate and momentum space, respectively. $N$ is the neutron number and $A$ is the mass number. $K_G(t)$ is the canonically conjugate momentum of $D_G(t)$. The evolution of the excited wave function to the final state is obtained by the EQMD model. From the Fourier transform of the second derivative of $D_G(t)$ with respect to time, i.e.,

$$D''(\omega) = \int_{t_0}^{t_{\max}} D''_G(t) e^{i\omega t} dt, \tag{10}$$

the dipole resonance strength of the system at excitation energy $E = \hbar\omega$ can be obtained by Eq. (11),

$$\frac{dP}{dE} = \frac{2e^2}{3\pi\hbar c^3 E}|D''(\omega)|^2, \tag{11}$$

where $dP/dE$ can be interpreted as the nuclear photoabsorption cross section.

Also, the GDR cross section can be obtained by calculating the nuclear response to external excitation. To describe an excitation of an external dipole field, the dipole operator can

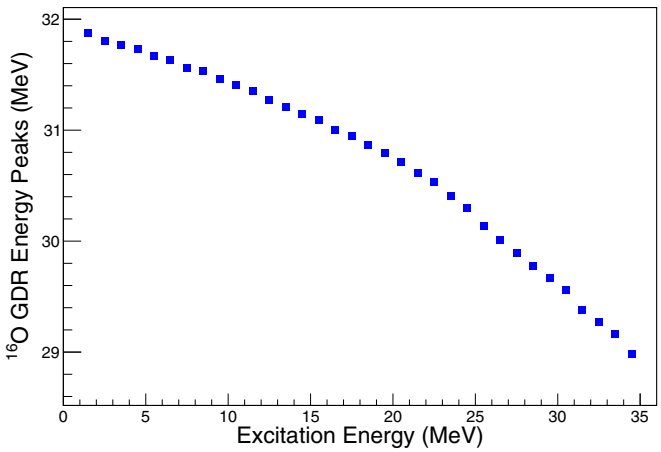


FIG. 1. Dependence of $^{16}$O GDR energy peaks on excitation energy.

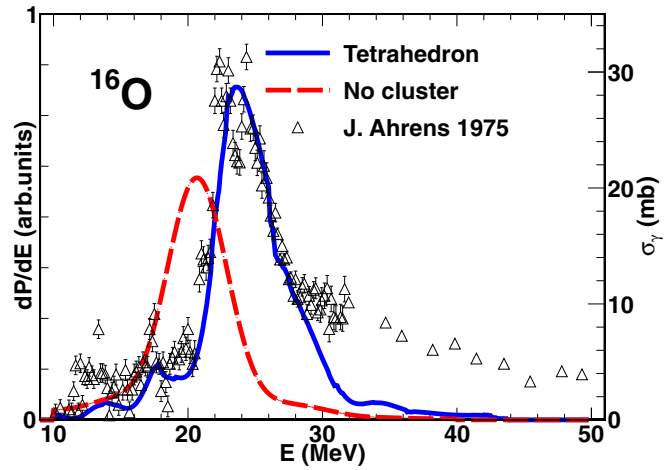


FIG. 2. Comparison of the GDR calculation for $^{16}$O against experimental data (nuclear photoabsorption cross section on the oxygen target) in Ref. [54] (Ahrens 1975, empty triangles, scaled by the right $y$ axis). Solid blue line: tetrahedral $\alpha$ cluster state. Long-dashed red line: noncluster state.

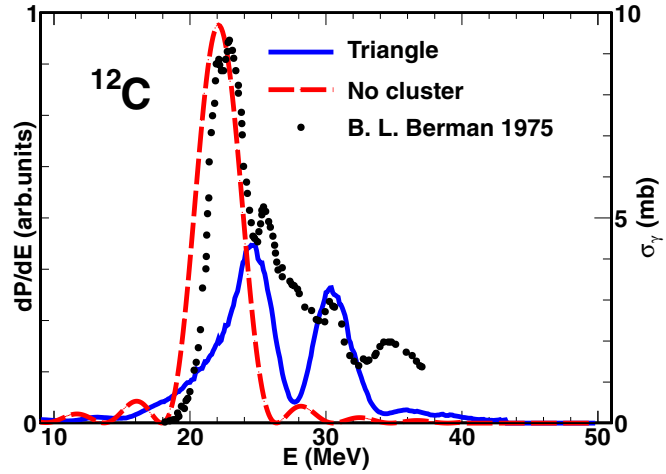


FIG. 3. Comparison of the GDR calculation for $^{12}$C against experimental data in Ref. [18] (Berman 1975, black dots, scaled by the right $y$ axis). Solid blue line: triangle $\alpha$ cluster state. Long-dashed red line: noncluster state.

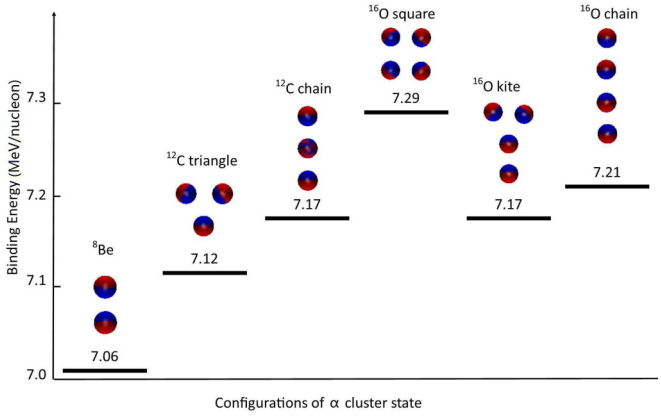


FIG. 4. Average binding energy for different $\alpha$ cluster structures around the threshold of $n\alpha$ breakup.

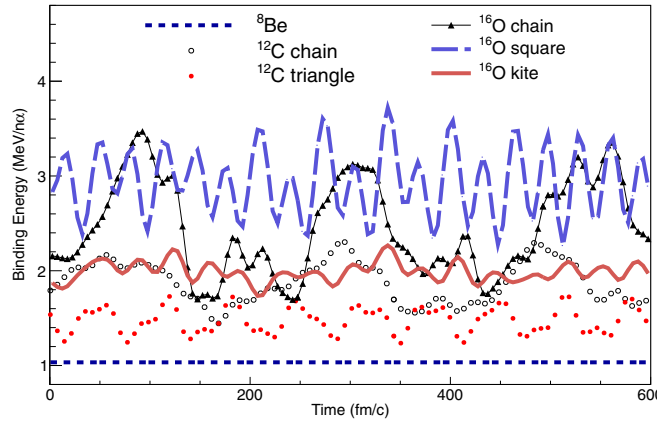


FIG. 6. Time evolutions of binding energy among $\alpha$ clusters for different configurations.

be written as

$$\mathbf{R} = \sum_i \left( \frac{N}{A} \mathbf{Pr}_i - \frac{Z}{A} \mathbf{Ne}_i \right) \mathbf{r}, \tag{12}$$

where $i$ indexes all nucleons in the nucleus, $N$ is the neutron number, $P$ is the proton number, and $A$ is the mass number. **Pr** and **Ne** are the projection operators for protons and neutrons, respectively. The dipole excitation can be written as an additional perturbative component to the Hamiltonian,

$$H' = \mathbf{R} \varepsilon \delta(t), \tag{13}$$

where $\varepsilon$ is an arbitrary small value, and $\delta P$ is the variation of momentum. The system wave function can be written as

$$\begin{aligned} &|\Psi(t=0)\rangle \\ &= \exp\left[ -i \int H' dt \right] |\Psi(0)\rangle \\ &= \exp\left[ -i \frac{r}{\hbar} \sum_i \Delta P \left( \sqrt{\frac{N}{AZ}} \widehat{\mathrm{Pr}_i} - \sqrt{\frac{Z}{AN}} \widehat{Ne_i} \right) \right] |\Psi(0)\rangle, \end{aligned} \tag{14}$$

with $\varepsilon$ being calculated by

$$\varepsilon = \frac{\Delta P}{\hbar} \sqrt{\frac{A}{NZ}}. \tag{15}$$

From linear response theory, the response of the dipole operator can be written as

$$S(\hat{R}) = \langle \hat{R} \rangle \frac{\hbar}{\Delta P \sqrt{A/(NZ)}}, \tag{16}$$

$$-\mathrm{Im} S(\hat{R}) = \sum_n |\langle n|\hat{R}|0\rangle|^2 \delta(\omega - \omega_n), \tag{17}$$

where $n$ indexes different excited states. Since evolution of the excited wave function to the final state can be obtained by the EQMD model, Eq. (18) shows the sum rule,

$$\begin{aligned} &\sum_n [\langle n|\hat{R}|0\rangle^2 \delta(\omega - \omega_n)] \\ &= -\mathrm{Im} \frac{\hbar}{\pi \Delta P \sqrt{A/(NZ)}} \int_0^\infty \langle \psi(t)|\hat{R}|\psi(t)\rangle e^{i\omega t} dt. \end{aligned} \tag{18}$$

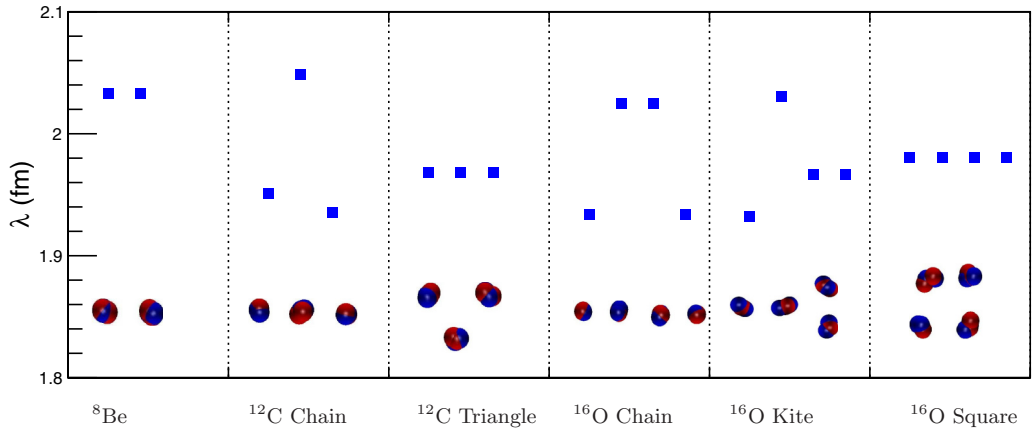


FIG. 5. Width of Gaussian wave packets in different clustering states. Blue and red bubbles above the horizontal axis are different configurations of $^8$Be, $^{12}$C, and $^{16}$O. Blue square marks are $\lambda$'s of wave packets for different clusters, scaled by the vertical axis.

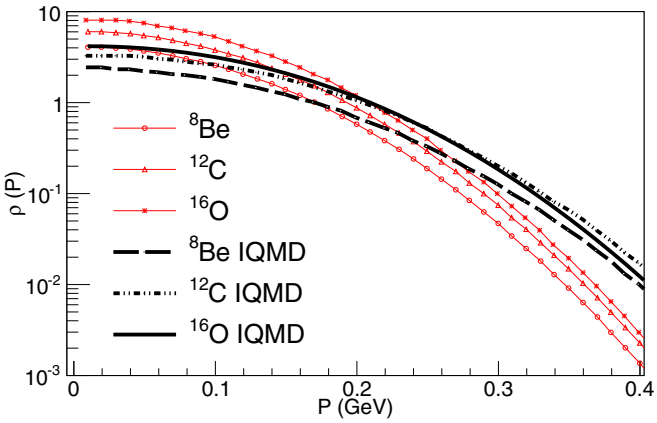


FIG. 7. Momentum distributions of different nuclei in the EQMD model and standard isospin-dependent quantum molecular dynamics (IQMD) model. Black lines show momentum distributions in a standard IQMD model and the red line with marks represents the EQMD model's results.

For $E1$ excitation, the cross section can be expressed as

$$\sigma(\omega) = 4\pi\alpha \frac{\hbar\omega}{\Delta P\sqrt{A/(NZ)}} \times \left(-\mathrm{Im}\int_0^\infty \langle\psi(t)|\hat{R}|\psi(t)\rangle e^{i\omega t}dt\right), \quad (19)$$

where $\omega$ is excitation energy and $\alpha$ is the fine structure constant.

It is confirmed that the two ways of calculating GDR spectra come to the same result. The following calculations are obtained by the response function method. In EQMD calculations for dipole oscillations of light nuclei, the system's response is not of perfect linearity. The positions of peaks of GDR spectra are dependent on oscillation energy (Fig. 1): the higher the excitation energy, the lower the peak of GDR. Since the excitation energy of GDR is usually in the range of 10 to 40 MeV, the width of GDR spectrum shifting is about 2 MeV. Because of the nonlinearity of response, which should be considered, we introduce a new normalization method [Eq. (20)] to take the width into account:

$$\frac{dP}{dE}_{\mathrm{norm}} = \frac{dP/dE}{\int_0^\infty (dP/dE)dE}. \quad (20)$$

In realistic calculations, the normalized $dP/dE$ is calculated in the excitation energy region of 8–35 MeV, which includes almost all the physically relevant GDR peaks.

In our calculations, no boundary of grids is used, so the Fourier transform, Eq. (10), does not induce spurious effects [53]. Because of the absence of decay channels, the damping of collective motions is not reasonable. In this context, the integration time of the Fourier transform should be cut according to experiments, and here 600 fm/$c$ is a reasonable selection. The finite integration time will bring additional spreading to the GDR spectrum; however, the spreading is less than 1 MeV, which is less than the width of GDR spectrum.

To get an accurate cross section of giant modes, the high order effect beyond mean-field pairing correlations and a more accurate description of continuum states are needed. However, in our result, $dP/dE$ is an arbitrary unit. A smoothing parameter $\Gamma = 2$ MeV is applied, when the $dP/dE$ spectrum is displayed.

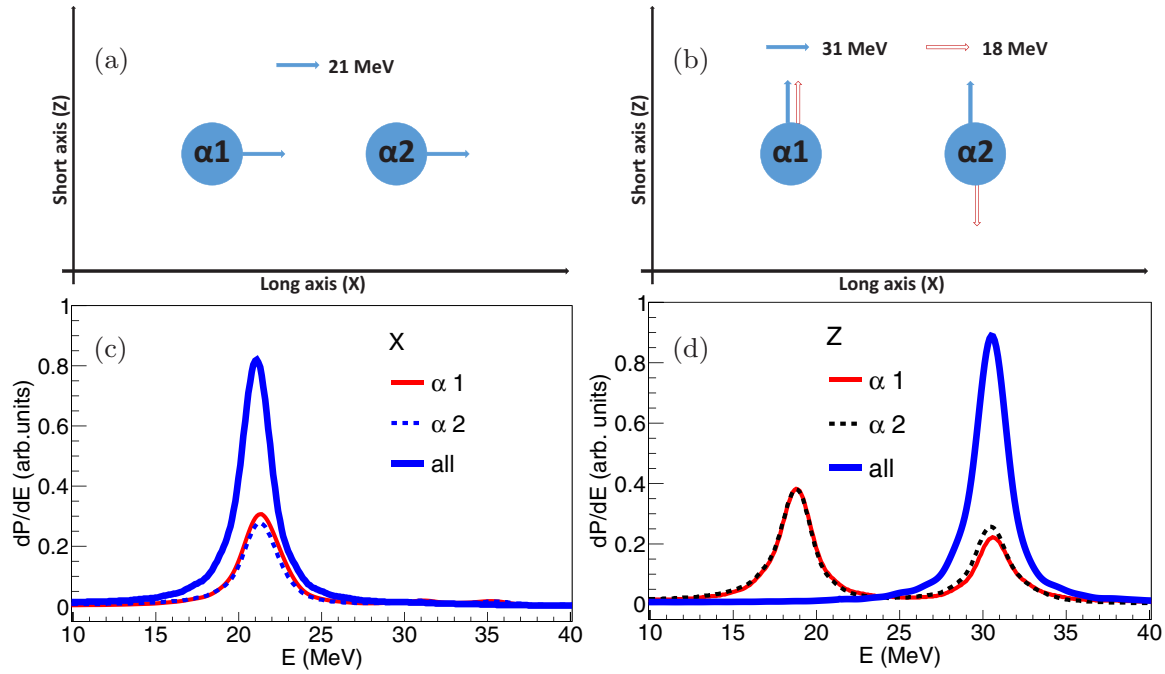


FIG. 8. Coherence of $^{8}$Be dipole motion. Panels (a) and (c) show the coherence of motion along the long axis. Panels (b) and (d) show the coherence of motion along the short axis. Arrows in (a) and (b) indicate the phase of oscillations at different frequencies.

## III. RESULTS AND DISCUSSION

### A. α cluster in ground states

In the EQMD model, the $^{16}$O ground state is obtained at a binding energy of 7.82$A$ MeV, which is close to the experimental binding energy, 7.98$A$ MeV, and consists of four $\alpha$'s with a tetrahedral configuration. The tetrahedral four-$\alpha$ configuration in the $^{16}$O ground state is also supported by an *ab initio* calculation by Epelbaum *et al.* [36] using nuclear chiral effective field theory. A recent covariant density functional theory calculation also shows a regular tetrahedral four-$\alpha$ configuration in the $^{16}$O ground state [29]. The noncluster $^{16}$O ground state in EQMD can be obtained with a wave packet width of 4.2–4.3 fm for all the nucleons. This width is much wider than that of nucleons in cluster states, in which all the nucleons have a width of just 1.9–2.1 fm. So the independent and variable wave packet width for each nucleon plays a crucial role on clustering, which is a distinct advantage of EQMD. Figure 2 shows the GDR results of noncluster and cluster $^{16}$O ground states, together with the experimental data in Ref. [54]. The GDR of the noncluster ground state cannot reproduce the data and the centroid is 4 MeV lower than the centroid of the main peak of the data. In contrast, the GDR of the tetrahedral configuration can reproduce the data well. So the tetrahedral four-$\alpha$ configuration in initialization is reasonable and the procedure used to calculate the GDR is reliable. For $^{12}$C, the noncluster ground state is also obtained, in which the wave packet widths of all the nucleons range from 3.5 to 3.6 fm. Figure 3 shows a comparison between the calculated result of $^{12}$C and the data. The noncluster ground state can reproduce the shape of the low energy peak quite well with only about 1 MeV centroid shift. The centroids of high energy small peaks can be obtained from the triangle $^{12}$C ground state. It is reasonable to infer that the ground state of $^{12}$C is a multiconfiguration mixing of shell-model-like and $\alpha$ cluster configurations, which is consistent with the calculations of AMD [55] and FMD [26] models.

### B. α cluster configurations around threshold of $n\alpha$ breakup

In th EQMD model framework, $^{8}$Be at ground state has $\alpha$ cluster structure. It consists of two $\alpha$ clusters, with 7.06$A$ MeV binding energy. $^{12}$C has two possible $\alpha$ cluster structures (Fig. 4). One is the triangle structure, with three $\alpha$ clusters forming a regular triangle shape. Its binding energy is 7.12$A$ MeV, a little bigger than that of $^{8}$Be. The other is the chain structure, with a binding energy of 7.17$A$ MeV, which means that the chain structure formed by three $\alpha$ clusters is more stable than the triangle structure. Similar to other theoretical predictions, $\alpha$ cluster states of light nuclei are shown, around the threshold energy, to decay into free $\alpha$ particles. In the EQMD result, $^{8}$Be is the closest to the threshold, and other $\alpha$ cluster states inside heavier nuclei have bigger binding energy than the threshold. For a nucleus with different $\alpha$ cluster states, the binding energies of different cluster states differ very little from each other, which indicates different energy levels. The $^{16}$O $\alpha$ cluster states have three structures, with bigger binding energies (than those of $^{8}$Be and $^{12}$C $\alpha$ cluster states) of 7.29$A$, 7.17$A$, and 7.21$A$ MeV for the square, kite, and chain structures respectively. Consequently, the most stable $\alpha$ cluster structure for $^{16}$O is square, and then the chain structure. The kite is the most unstable structure. The excitation energy shown in Fig. 4 for $^{12}$C and $^{16}$O is very near the predicted threshold energy in the Ikeda diagram [3]. We have checked that our results are not sensitive to the tiny binding energy difference, just sensitive to the geometric configurations of clusters.

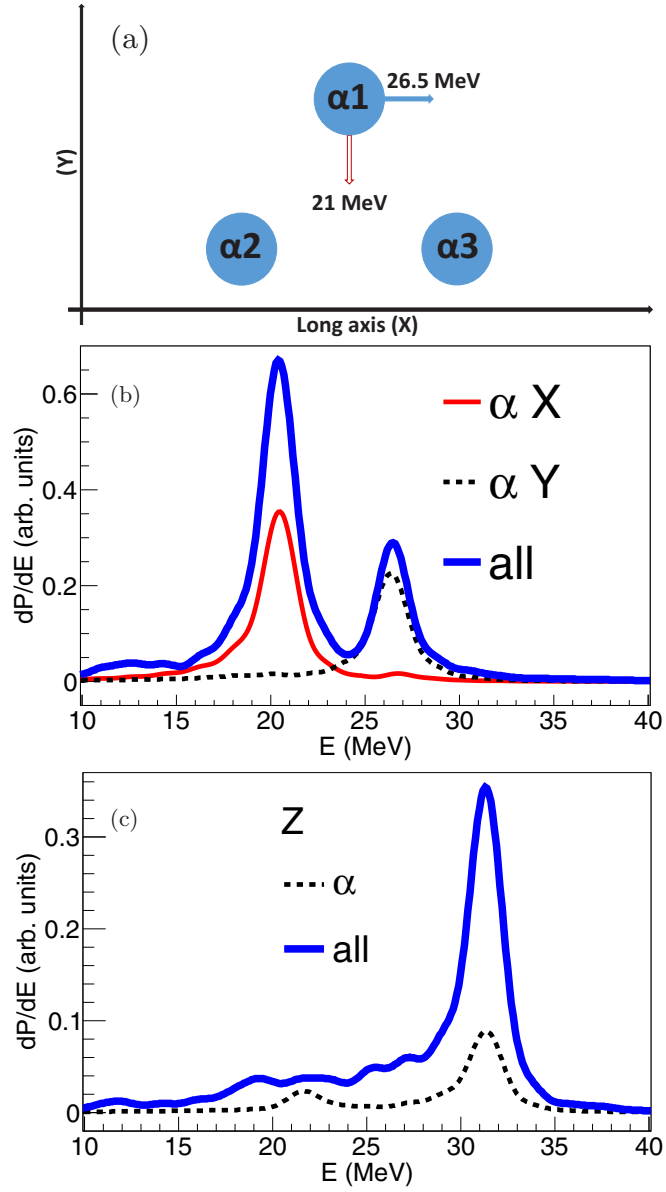


FIG. 9. Coherence of $^{12}$C triangle structure dipole motion. Panels (a) and (b) show the coherence of motion along the long axis. Panel (c) shows the coherence of motion along the short axis. Arrows in (a) indicate the phase of oscillations at different frequencies.

$\alpha$ cluster structures that are less symmetrical, like the $^{12}$C chain structure compared to the triangle structure, are more stable. This property indicates that $\alpha$ clusters in the $^{12}$C chain structure state play different roles. For instance, the $\alpha$ cluster at the center of $^{12}$C chain structure has a larger Gaussian wave

packet width, which can help to hold the $\alpha$ clusters at both ends of the chain. The $\lambda_i$ of nucleons in different $\alpha$ clusters are shown in Fig. 5. As one can see in $^{16}$O chain structure and kite structure, $\alpha$ clusters at the center of a nucleus have larger Gaussian wave packet widths than outer ones.

In the EQMD framework, the binding energy of $\alpha$ clusters in nuclei is smaller than that of free $\alpha$ particles. For $^{8}$Be, the calculated internal binding energy of the $\alpha$ cluster is 27.2 MeV, which is a little less than the experimental result (28.3 MeV) for the free $\alpha$ particle. Considering that the binding energy of the $^{8}$Be system is 7.06$A$ MeV, one knows that the binding energy between two $\alpha$ clusters is 1.02 MeV/$\alpha$. For $^{12}$C and $^{16}$O, the binding energy among $\alpha$ clusters shows larger values. Under time evolution, those binding energies will oscillate periodically (see Fig. 6). In fact, the $^{8}$Be binding energy between two $\alpha$ clusters oscillates, though with very small amplitude ($<$ 0.01 MeV). Figure 6 shows that the periods are very different and are sensitive to $\alpha$ cluster structure, and every oscillation consists of multiple frequencies. For the $^{16}$O chain structure, more than two periods are within a difference of $>$200 fm/$c$. The oscillation of binding energy indicates that energy flows into and out of the $\alpha$ clusters periodically.

The momentum distribution of cluster states differs greatly from that normal nuclei at ground state. Figure 7 shows momentum distributions of $^{8}$Be, $^{12}$C, and $^{16}$O. The red data points are clustering state results calculated in the EQMD model, where the black lines are the nonclustering state results calculated in the IQMD model. The momentum distribution is not sensitive to different structures of $\alpha$ clusters. As shown by the red marked lines, the $^{12}$C chain structure and triangle structure give the same result, and the $^{16}$O chain, square, and kite structures also give the same results. One can see from Fig. 7 that, in the low momentum region, clustering nuclei have higher values of momentum distribution than nonclustering nuclei, while this reverses in the high momentum region.

To calculate the GDR spectrum, one can give the nucleus a boost to obtain the dipole oscillation, or simulate a Coulomb excitation with a heavier nucleus. The two methods give the same result. But the first method gives no information about the difference between $\alpha$ clusters in a nucleus. To discuss the dipole motion's coherence of different $\alpha$ clusters in a nucleus, the following results of this section are obtained by simulations of clustering nuclei as projectiles hitting $^{40}$Ca as target. In detail, the impact parameter is 20 fm, and the projectiles are 100 MeV in incident energy. The systems evolve, stopping at 600 fm/$c$. The length of time will affect the GDR spectrum width in EQMD calculations: the shorter the calculation time, the wider the spectrum obtained. Therefore, the time should be greater than 300 fm/$c$, to avoid a too wide GDR spectrum width. Because the oscillations excited by Coulomb reaction are of small amplitude, the peaks of GDR spectra in this article shift 1 MeV toward high energy compared with our previous results [24]. Another point that should be mentioned here is that the excited energy of the following results are based on cluster states which are all low-lying states, and are different from the excited energy mentioned in Sec. III A (Figs. 2 and 3) which are based on ground states.

### C. $^{8}$Be dipole oscillation

As a collective motion of nucleons, GDR will be affected sensitively by nuclear exotic structures. $\alpha$ clusters will split and complicate the GDR spectrum. To discuss how $\alpha$ clusters affect collective motions, we use $^{8}$Be as the simplest example. Figure 8 shows the GDR spectrum of $^{8}$Be. The two peaks at 21 and 31 MeV are contributed by the long and the

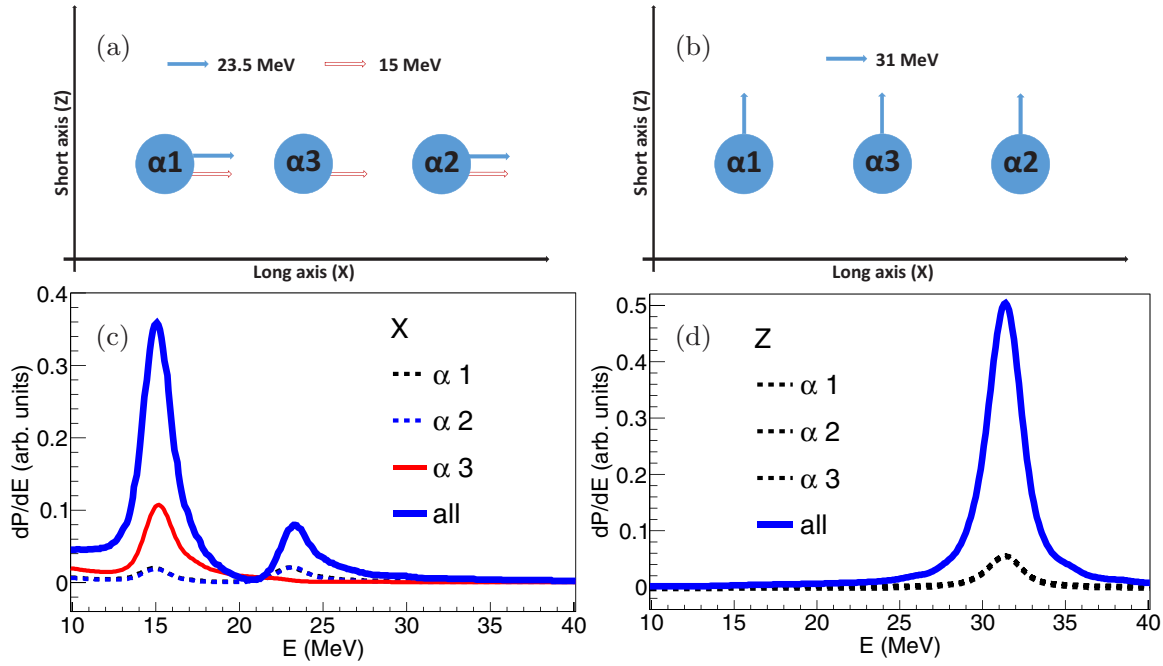


FIG. 10. Coherence of $^{12}$C chain structure dipole motion. Panels (a) and (c) show the coherence of motion along the long axis. Panels (b) and (d) show the coherence of motion along the short axis. Arrows in (a) and (b) indicate the phase of oscillations at different frequencies.

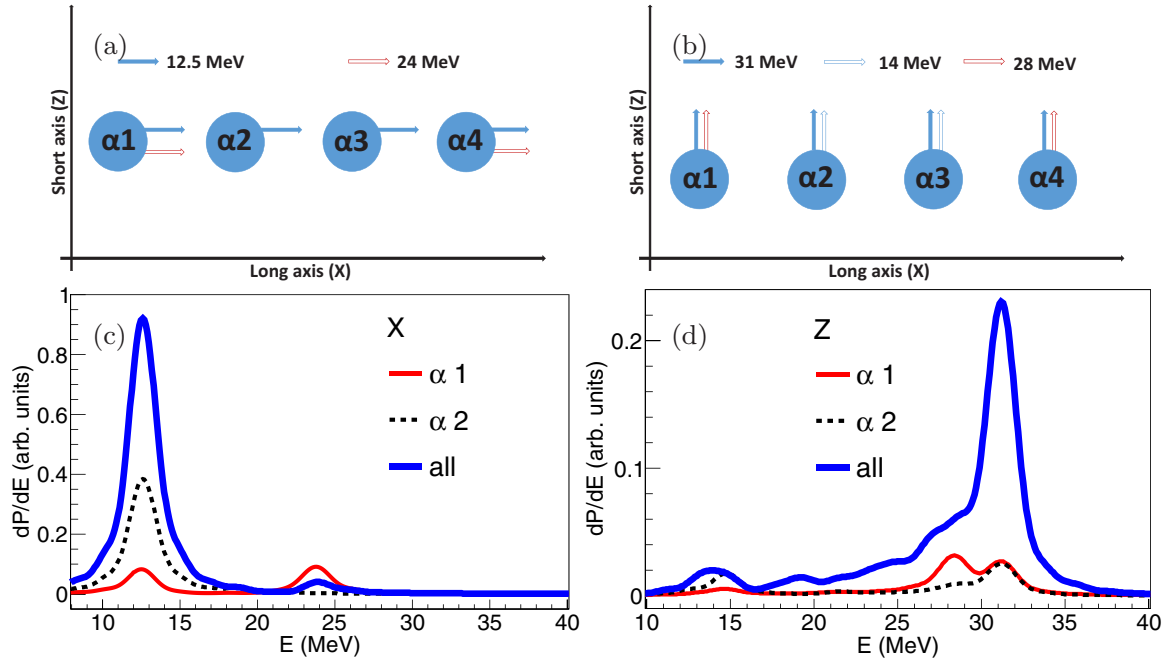


FIG. 11. Coherence of $^{16}$O chain structure dipole motion. (a) and (c) show the coherence of motion along the long axis. (b) and (d) show the coherence of motion along the short axis. Arrows in (a) and (b) indicate the phase of oscillations in different frequencies.

short axes of system, respectively. There exists a rule that the dipole oscillation frequency in any direction of a cluster system is inversely proportional to the length of the system's configuration. In Fig. 8, both $\alpha$ clusters have a single frequency in the long axis direction at 21 MeV with the same oscillation phase. It should be noted that the arrows drawn on the clusters do not indicate the motion direction of the whole $\alpha$ cluster, but represent the isovector dipole motion in the $\alpha$ cluster, in which the two protons move against the two neutrons. For example, in Fig. 8(b), the two filled blue arrows with the same direction mean that the two $\alpha$ clusters have the same direction of isovector dipole motion with the same oscillation phase; the two empty red arrows with opposite direction mean that the two $\alpha$ clusters have the same direction of isovector dipole motion but with the opposite oscillation phase. For this case, in the short axis direction, every $\alpha$ cluster has two frequencies, at 31 and 18 MeV. The oscillations of the two $\alpha$ clusters at 31 MeV are coherent with the same phase, while the peak at 18 MeV disappears when two $\alpha$ clusters are considered as a whole system. The oscillations with this frequency are coherent with opposite phase.

### D. $^{12}$C dipole oscillation

#### 1. $^{12}$C *triangle structure*

The $^{12}$C GDR spectrum with triangle structure gives three peaks, at 21, 26.5, and 31 MeV. For this configuration, the short axis is perpendicular to the plane determined by the triangle shape. In this direction, every $\alpha$ cluster has a main peak at 31 MeV and a small peak at 21.5 MeV. But the little peaks of different $\alpha$ clusters are noncoherent. So this peak does not show up in the whole system GDR spectrum. The frequency of 31 MeV is coherent, which gives a strong peak. In the long

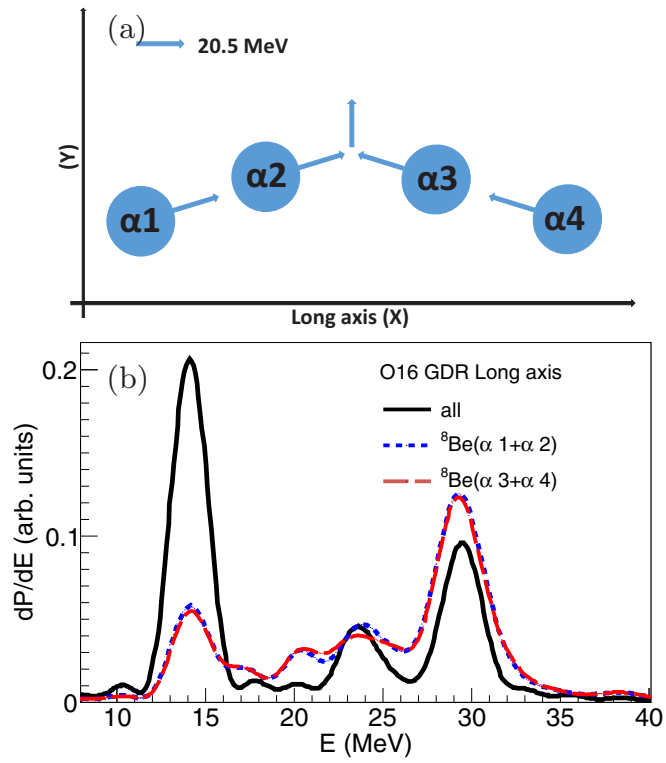


FIG. 12. $^{8}$Be substructure in $^{16}$O chain state. (a) gives the phase of oscillation and (b) shows the GDR spectra along the long axis. The peak at 20.5 MeV raised by substructure of $^{8}$Be (long dashed line and short dashed line) are subtracted coherently, so the total spectra (solid line) do not have peak at 20.5 MeV.

axis, every $\alpha$ cluster has two peaks, at 21 and 26.5 MeV. The 21 MeV peak is close to GDR peak of $^{8}$Be in the long axis and is supposed to be built by interaction of two $\alpha$ clusters. To check the components of peaks at 26.5 MeV, the long axis is rotated by $\pi/6$. As shown in Fig. 9, after rotation, the two components of 26.5 and 21 MeV are separated. The oscillating direction of 26.5 MeV frequency is parallel to the bottom line of the triangle shape. This frequency is proposed to be built by interaction among three $\alpha$ clusters.

### 2. $^{12}$C *chain structure*

The results of $^{12}$C with chain structure are shown in Fig. 10, with three components at 15, 23.5, and 31.5 MeV. The 31.5 MeV peak is along the short axis, and is contributed to equally by every $\alpha$ cluster, while the 15 MeV peak is contributed to mainly by the central $\alpha$ cluster. The $\alpha$ clusters at both ends contribute to it, though weakly. The central $\alpha$ cluster feels stronger three-$\alpha$ interaction than the two other-side $\alpha$ clusters. For the peak at 23.5 MeV, it is supposed to be built by three-$\alpha$ interaction like the triangle structure. This kind of three-$\alpha$ interaction is sensitive to the configuration of $\alpha$ clusters. The regular triangle structure shows stronger oscillation strength at the higher frequency of 26.5 MeV, andthe chain structure gives weak strength and lower frequency at 23.5 MeV. Because of the weak oscillations caused by Coulomb excitation, it does not show a peak around 21 MeV, which indicates the two-$\alpha$ interaction. In fact, when the dipole oscillation has larger strength, the triangle structure may degenerate into a $^{8}$Be substructure with an $\alpha$ bounded to it very weakly. Then it will give a peak around 21 MeV.

### 3. $^{16}$O *chain structure*

Figure 11 shows the spectrum of the short axis. The coherent peak locates at 31 MeV too. The $\alpha$ clusters at the ends of the chain structure appear at a frequency at 28.5 MeV, which is supposed to be a multi-$\alpha$-interaction effect. As the previous results do not show these peaks, it can be supposed to show up only when the oscillation strength is weak enough and the structure keeps a nearly regular linear chain. The same occurs at 14 MeV. It is a very small peak, and the oscillations are noncoherent, so its total strength is close to one $\alpha$ cluster. For the long axis, the main peak locates at 12.5 MeV, due to the mean field effect of the system. Its size is the largest of all nuclei and structures, hence it has the lowest frequency of all. Like the case of $^{12}$C chain structure, the $\alpha$ clusters at the center have the strongest oscillation strength. The peak

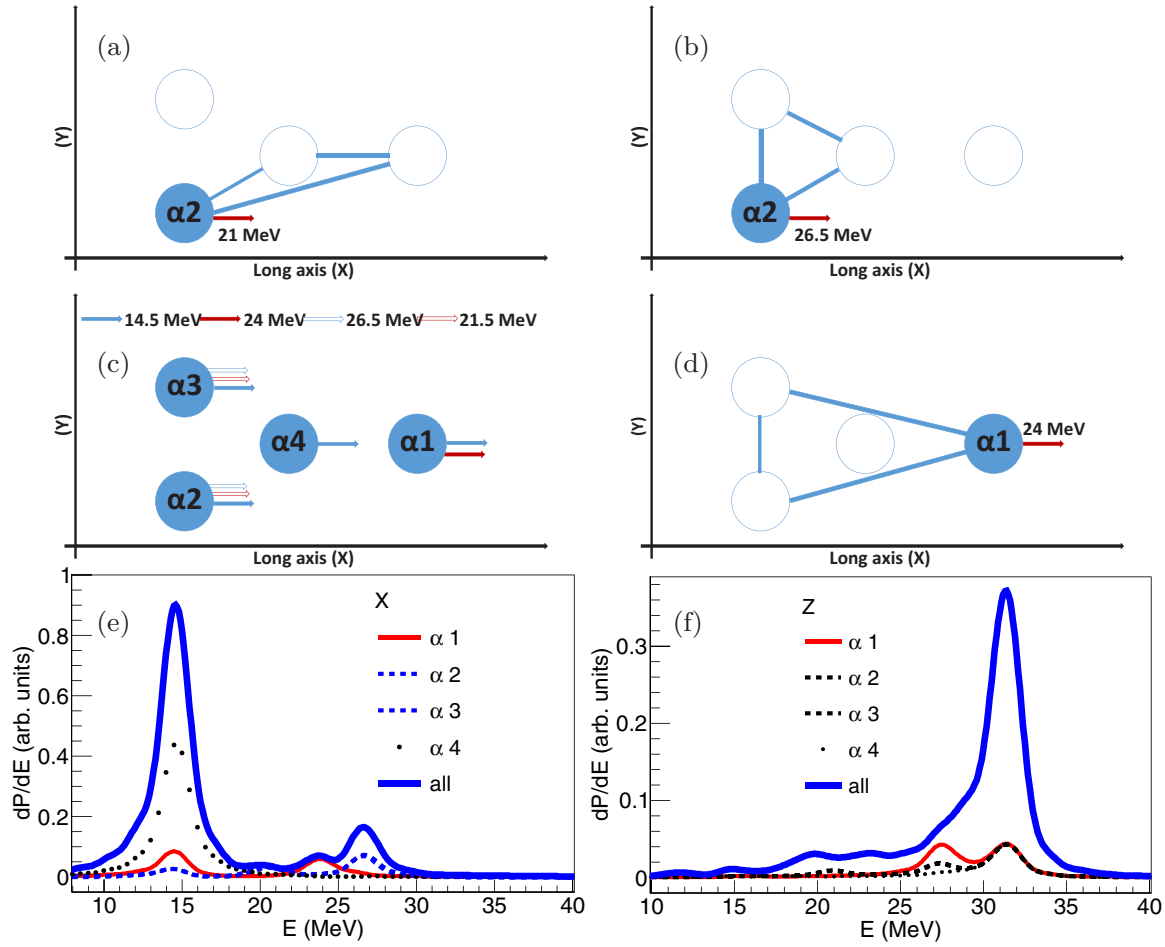


FIG. 13. Coherence dipole motion of $^{16}$O kite structure. (a), (b), and (d) Different oscillations caused by three-$\alpha$ substructure, with small peaks at 20–30 MeV. (c) and (e) Coherence along the long axis. (f) GDR spectra along the short axis.

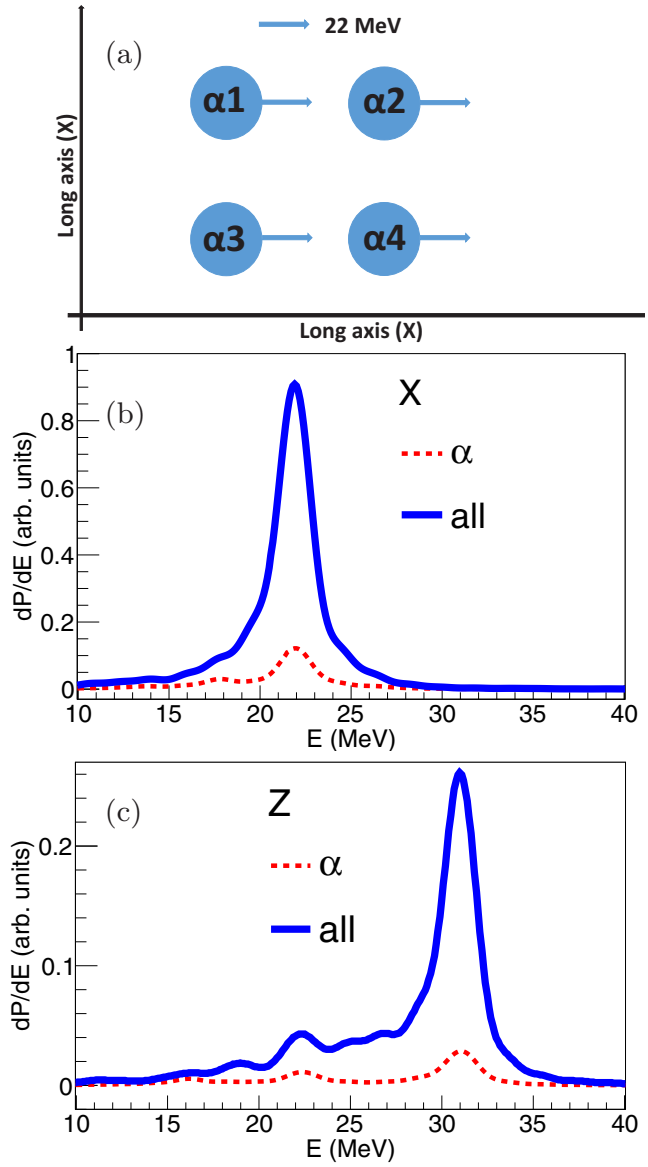


FIG. 14. Coherence of $^{16}$O square structure dipole motion. (a) and (b) The coherence of motion along the long axis. (c) Coherence of motion along the short axis. Arrows in (a) indicate the phase of oscillation.

at 24 MeV indicates that $\alpha$ clusters at the chain ends feel a three-$\alpha$-interaction like the $^{12}$C chain and triangle structures. But oscillation of the two $\alpha$ clusters is noncoherent, so the total GDR strength is not stronger than one $\alpha$ cluster. Figure 12 shows that the GDR spectrum of $^{16}$O chain structure is a little bent. If the chain is considered as two $^{8}$Be subsystems, each $^{8}$Be will show a peak around 20.5 MeV in the GDR spectrum. But the two subsystems are coherent with opposite phase, so the peak disappears in the total GDR spectrum.

#### 4. $^{16}$O *kite structure*

The $^{16}$O kite structure is the most complicated $^{16}$O structure, and is more complicated than the $^{12}$C cluster states discussed above. It can be regarded as one triangle $^{12}$C added with a weakly bound $\alpha$ located at one of the vertices of the triangle structure. The wave packets of nucleons in the central $\alpha$ cluster are larger than nucleons in other $\alpha$ clusters, including the $^{12}$C triangle state. This is the way to keep the additional $\alpha$ cluster bounded. Figure 13 shows the GDR spectrum in the short axis; all peaks are similar to the $^{16}$O chain structure, without the peak at 14 MeV. In the long axis, each $\alpha$ cluster behaves very differently. The GDR peak at 14.5 MeV is determined by the mean field effect, with the central $\alpha$ cluster contributing the most of all the $\alpha$ clusters in triangle subsystem. In other words, the weakly bounded $\alpha$ clusters contribute the lowest. The three-$\alpha$ interaction is dependent on the structures of the related $\alpha$ clusters. The $^{16}$O kite structure can be decomposed into three kinds of triangle structures. As shown in Fig. 13, $\alpha$ 1 gives a peak at 24 MeV, which is the effect of triangle 1 structure. This frequency is lower than that of the $^{12}$C triangle state, and higher than that of the $^{12}$C chain state, due to difference of the triangle structures. $\alpha$'s 2 and 3 give peaks at 26.5 and 21.5 MeV, respectively. The 26.5 MeV peak is similar to that of the $^{12}$C triangle state, because of is the similar triangle structures. $\alpha$ 2 (or 3), $\alpha$ 4, and $\alpha$ 1 make up an obtuse triangle structure. This special structure makes $\alpha$ 2 and 3 give a peak at lower energy, so the peak at 21.5 MeV is not caused by the $^{8}$Be subsystem.

#### 5. $^{16}$O *square structure*

The $^{16}$O square structure is a comparatively simple structure. As shown in Fig. 14, the short axis peak is at 31 MeV and the long axis peak is at 22 MeV. Because this state has the highest binding energy and the structure enhances three $\alpha$

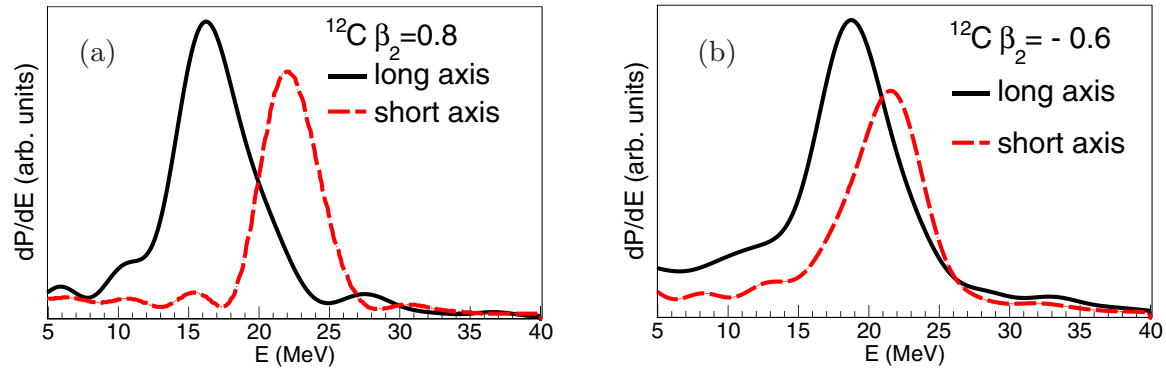


FIG. 15. GDR spectra split by deformation. (a) Deformation with $\beta_2 = 0.8$; (b) deformation with $\beta_2 = -0.6$.

interaction, the energy peak in the long axis is the highest of all states.

### E. The difference of GDR spectrum between $\alpha$ cluster states and deformation

The calculated GDRs of $^{12}$C in positive or negative $\beta_2$, without clustering, are shown in Fig. 15. However, these $^{12}$C samples are initialized manually. The split between two peaks is much smaller than the split of GDR with clustering. The missing 30 MeV peak is a significant difference in comparison with the $\alpha$ cluster states. This is true for both prolate and oblate deformations.

The homogeneous prolate or oblate ellipsoid, which has two collective structure degrees of freedom, usually can have two obvious peaks, corresponding to the long and short axes, respectively, whereas a clustering GDR spectrum with multiple peaks has several collective degrees of freedom. The fragmented response function is a complicated coherent result of strong interference between $\alpha$'s, which counteract or strengthen each other. The GDR peak around 30 MeV is a reliable proof to confirm the existence of $\alpha$ clusters in light nuclei.

There are obvious substructures in GDR, such as similar GDRs of $^{8}$Be and triangle $^{12}$C, that appear as substructure in GDRs of chain $^{12}$C and kite $^{16}$O, respectively. This distinct feature of GDR can be taken as a strong signal which is different from the normal prolate or oblate deformation in light nuclei.

## IV. CONCLUSIONS

In conclusion, the advantage and results of the EQMD model to describe cluster states and a calculation method of isovector nuclear GDR are discussed. Properties of ground states and $\alpha$ cluster states in light nuclei are discussed with an extended QMD model. $^{8}$Be at ground state consists of two $\alpha$ clusters. For $^{12}$C and $^{16}$O cluster states, clusters form different configurations. The average binding energies of $^{12}$C and $^{16}$O cluster states, around threshold energy for the decay into free $\alpha$ particles, are slightly bigger than that of $^{8}$Be at 7.07$A$ MeV. For cluster states, the binding energy between $\alpha$ clusters is studied, which oscillates in several frequencies. So, energy flows into and out of the clusters periodically. The dynamic Gaussian wave packets' width is important for a QMD model to describe nuclear $\alpha$ cluster states. For different $\alpha$ clusters in a nucleus, the central ones have larger width and the outer ones have smaller width. The momentum distribution of $\alpha$ cluster states differs greatly from the that of nuclei in the standard QMD model.

Collective excitation of $\alpha$ cluster states shows interesting phenomena. The giant dipole resonances depends on geometric configuration of $\alpha$ clusters in a nucleus. The Coulomb excitation process is applied to study the resonance rule of different $\alpha$ clusters. The dipole oscillation frequency in any direction of a cluster's system is inversely proportional to the length of the system configuration. As the simplest system of a cluster state, $^{8}$Be has one GDR peak at 31 MeV oscillating perpendicular the long symmetrical axis of two $\alpha$ clusters and another peak at 21 MeV oscillating along the long axis. The complicated behavior of collective oscillations for $^{12}$C and $^{16}$O $\alpha$ cluster states with different configurations are discussed in detail. These show that GDR spectra of clustered nuclei are sensitive to $\alpha$ cluster states and configurations.

## ACKNOWLEDGMENTS

This work was supported in part by the National Natural Science Foundation of China under Contracts No. 11421505, No. 11305239, and No. 11220101005 and by the Major State Basic Research Development Program in China under Contract No. 2014CB845401.

[1] W. Greiner, J. Y. Park, and W. Scheid, *Nuclear Molecules* (World Scientific, Singapore, 1995).
[2] W. von Oertzen, M. Freer, and Y. Kanada-En'yo, Phys. Rep. **432**, 43 (2006).
[3] K. Ikeda, N. Takigawa, and H. Horiuchi, Prog. Theor. Phys. Suppl. **E68**, 464 (1968).
[4] D. M. Brink and J. J. Castro, Nucl. Phys. A **216**, 109 (1973).
[5] T. Yamada, Y. Funaki, H. Horiuchi, G. Röpke, P. Schuck, and A. Tohsaki, in *Cluster in Nuclei*, Vol. 2, edited by C. Beck, Lecture Notes in Physics 848 (Springer-Verlag, Berlin, 2012).
[6] M. Girod and P. Schuck, Phys. Rev. Lett. **111**, 132503 (2013).
[7] G. Röpke, N.-U. Bastian, D. Blaschke, T. Klähn, S. Typel, and H. H. Wolter, Nucl. Phys. A **897**, 70 (2013).
[8] C. J. Horowitz and A. Schwenk, Nucl. Phys. A **776**, 55 (2006).
[9] J. B. Natowitz, G. Röpke, S. Typel *et al.*, Phys. Rev. Lett. **104**, 202501 (2010).
[10] L. Qin, K. Hagel, R. Wada *et al.*, Phys. Rev. Lett. **108**, 172701 (2012).
[11] F. Hoyle, Astrophys. J. Suppl. Ser. **1**, 121 (1954).
[12] A. S. Umar, J. A. Maruhn, N. Itagaki, and V. E. Oberacker, Phys. Rev. Lett. **104**, 212503 (2010).
[13] T. Ichikawa, J. A. Maruhn, N. Itagaki, and S. Ohkubo, Phys. Rev. Lett. **107**, 112501 (2011).
[14] J.-P. Ebran, E. Khan, T. Nikšić, and D. Vretenar, Nature (London) **487**, 341 (2012).
[15] M. Freer, Rep. Prog. Phys. **70**, 2149 (2007).
[16] Y. Funaki, M. Girod, H. Horiuchi, G. Röpke, P. Schuck, A. Tohsaki, and T. Yamada, J. Phys. G **37**, 064012 (2010).
[17] V. D. Efros, W. Leidemann, and G. Orlandini, Phys. Rev. Lett. **78**, 4015 (1997).
[18] B. L. Berman and S. C. Fultz, Rev. Mod. Phys. **47**, 713 (1975).
[19] M. N. Harakeh and A. Van der Woode, *Giant Resonances: Fundamental High-Frequency Modes of Nuclear Excitation* (Oxford University Press, Oxford, 2001), Vol. 24.
[20] D. Pandit, S. Mukhopadhyay, S. Bhattacharya *et al.*, Phys. Rev. C **81**, 061302 (2010).
[21] D. Pandit, B. Dey, D. Mondal, S. Mukhopadhyay, S. Pal, S. Bhattacharya, A. De, and S. R. Banerjee, Phys. Rev. C **87**, 044325 (2013).

[22] R. A. Eramzhyan, B. S. Ishkhanov, I. M. Kapitonov, and V. G. Neudatchin, Phys. Rep. **136**, 229 (1986).
[23] T. Yamagata, S. Nakayama, H. Akimune *et al.*, Phys. Rev. C **69**, 044313 (2004).
[24] W. B. He, Y. G. Ma, X. G. Cao, X. Z. Cai, and G. Q. Zhang, Phys. Rev. Lett. **113**, 032506 (2014); W. B. He, X. G. Cao, Y. G. Ma *et al.*, Nucl. Techniques (in Chinese) **37**, 100511 (2014).
[25] Y. Chiba, M. Kimura, and Y. Taniguchi, Phys. Rev. C **93**, 034319 (2016).
[26] M. Chernykh, H. Feldmeier, T. Neff, P. von Neumann-Cosel, and A. Richter, Phys. Rev. Lett. **98**, 032501 (2007).
[27] Y. Kanada-En'yo, M. Kimura, and A. Ono, Prog. Theor. Exp. Phys. **2012**, 01A202 (2012).
[28] T. Furuta, K. H. O. Hasnaoui, F. Gulminelli, C. Leclercq, and A. Ono, Phys. Rev. C **82**, 034307 (2010).
[29] L. Liu and P. W. Zhao, Chin. Phys. C **36**, 818 (2012).
[30] D. J. Marín-Lámbarri, R. Bijker, M. Freer, M. Gai, Tz. Kokalova, D. J. Parker, and C. Wheldon, Phys. Rev. Lett. **113**, 012502 (2014).
[31] H. Morinaga, Phys. Lett. **21**, 78 (1966).
[32] P. W. Zhao, N. Itagaki, and J. Meng, Phys. Rev. Lett. **115**, 022501 (2015).
[33] A. Tohsaki, H. Horiuchi, P. Schuck, and G. Röpke, Phys. Rev. Lett. **87**, 192501 (2001).
[34] T. Suhara, Y. Funaki, B. Zhou, H. Horiuchi, and A. Tohsaki, Phys. Rev. Lett. **112**, 062501 (2014).
[35] W. Bauhoff, H. Schultheis, and R. Schultheis, Phys. Rev. C **29**, 1046 (1984).
[36] E. Epelbaum, H. Krebs, T. A. Lähde, D. Lee, Ulf-G. Meißner, and G. Rupak, Phys. Rev. Lett. **112**, 102501 (2014).
[37] R. Bijker and F. Iachello, Phys. Rev. Lett. **112**, 152501 (2014).
[38] T. Yamada, Y. Funaki, T. Myo, H. Horiuchi, K. Ikeda, G. Röpke, P. Schuck, and A. Tohsaki, Phys. Rev. C **85**, 034315 (2012).
[39] S. P. G. Chappell, D. L. Watson, S. P. Fox *et al.*, Phys. Rev. C **51**, 695 (1995).
[40] S. Marsh and W. D. M. Rae, Phys. Lett. B **180**, 185 (1986).
[41] B. Zhou, Y. Funaki, H. Horiuchi, Z. Ren, G. Röpke, P. Schuck, A. Tohsaki, C. Xu, and T. Yamada, Phys. Rev. Lett. **110**, 262501 (2013).
[42] W. Broniowski and E. Ruiz Arriola, Phys. Rev. Lett. **112**, 112501 (2014).
[43] J. Aichelin, Phys. Rep. **202**, 233 (1991).
[44] Y. Kanada-En'yo and M. Kimura, Phys. Rev. C **72**, 064301 (2005); Y. Kanada-En'yo, M. Kimura, F. Kobayashi, T. Suhara, Y. Taniguchi, and Y. Yoshida, Nucl. Sci. Techniques **26**, S20501 (2015).
[45] H. L. Wu, W. D. Tian, Y. G. Ma, X. Z. Cai, J. G. Chen, D. Q. Fang, W. Guo, and H. W. Wang, Phys. Rev. C **81**, 047602 (2010).
[46] C. Tao, Y. G. Ma, G. Q. Zhang, X. G. Cao, D. Q. Fang, and H. W. Wang, Phys. Rev. C **87**, 014621 (2013); C. Tao, Y. G. Ma, G. Q. Zhang, X. G. Cao, D. Q. Fang, H. W. Wang, and J. Xu, *ibid.* **88**, 064615 (2013); C. Tao, Y. G. Ma, G. Q. Zhang, X. G. Cao, D. Q. Fang, and H. W. Wang, Nucl. Sci. Techniques **24**, 030502 (2013); S.-Q. Ye, X.-Z. Cai, D.-Q. Fang, Y.-G. Ma, and W.-Q. Shen, *ibid.* **24**, 030501 (2014).
[47] X. G. Cao, G. Q. Zhang, X. Z. Cai, Y. G. Ma, W. Guo, J. G. Chen, W. D. Tian, D. Q. Fang, and H. W. Wang, Phys. Rev. C **81**, 061603(R) (2010); X. G. Cao, X. Z. Cai, Y. G. Ma, D. Q. Fang, G. Q. Zhang, W. Guo, J. G. Chen, and J. S. Wang, *ibid.* **86**, 044620 (2012).
[48] T. Maruyama, K. Niita, and A. Iwamoto, Phys. Rev. C **53**, 297 (1996).
[49] R. Wada, K. Hagel, J. Cibor, J. Li, N. Marie, W. Q. Shen, Y. Zhao, J. B. Natowitz, and A. Ono, Phys. Lett. B **422**, 6 (1998).
[50] S. S. Wang, X. G. Cao, T. L. Zhang, H. W. Wang, G. Q. Zhang, D. Q. Fang, C. Zhong, C. W. Ma, W. B. He, and Y. G. Ma, Nucl. Phys. Rev. **32**, 24 (2015).
[51] M. Goldhaber and E. Teller, Phys. Rev. **74**, 1046 (1948).
[52] V. Baran, M. Cabibbo, M. Colonna, M. Di Toro, and N. Tsoneva, Nucl. Phys. A **679**, 373 (2001).
[53] P. G. Reinhard, P. D. Stevenson, D. Almehed, J. A. Maruhn, and M. R. Strayer, Phys. Rev. E **73**, 036709 (2006).
[54] J. Ahrens, H. Borchert, K. H. Czock *et al.*, Nucl. Phys. A **251**, 479 (1975).
[55] Y. Kanada-En'yo, Phys. Rev. Lett. **81**, 5291 (1998).